The University of Osaka
Institutional Knowledge Archive

Title	Characterization and Reactivity Studies of Mononuclear Tetrahedral Copper(II)-Halide Complexes
Author(s)	Lan, Yang; Morimoto, Yuma; Shimizu, Ikuma et al.
Citation	Inorganic Chemistry. 2023, 62(27), p. 10539-10547
Version Type	AM
URL	https://hdl.handle.net/11094/94621
rights	This document is the Accepted Manuscript version of a Published Work that appeared in final form in Inorganic Chemistry, © American Chemical Society after peer review and technical editing by the publisher. To access the final edited and published work see https://doi.org/10.1021/acs.inorgchem.3c00320.
Note	

The University of Osaka Institutional Knowledge Archive : OUKA

https://ir.library.osaka-u.ac.jp/

The University of Osaka

Characterization and Reactivity Studies of Mononuclear Tetrahedral Copper(II)-halide Complexes

Yang Lan, Yuma Morimoto, Ikuma Shimizu, Hideki Sugimoto, and Shinobu Itoh*

Department of Molecular Chemistry, Division of Applied Chemistry, Graduate School of Engineering, Osaka University, 2-1 Yamada-oka, Suita, Osaka 565-0871, Japan
*Email: shinobu@chem.eng.osaka-u.ac.jp

ABSTRACT: Structures, physicochemical properties, and reactivity of the whole series of copper(II)-halide complexes ($\mathbf{1^X}$; X = F, Cl, Br, and I) were examined using TMG_3tach tridentate supporting ligand consisting of *cis,cis*-1,3,5-triaminocyclohexane (tach) and *N,N,N′,N′*-tetramethylguanidine (TMG). The tach ligand framework with the bulky and strongly electron donating TMG substituents enforces the copper(II) complexes to take a tetrahedral geometry as inferred from the electron paramagnetic resonance (EPR) spectra exhibiting relatively large g_z and small A_z values. The electronic absorption spectra of $\mathbf{1^X}$ agreed with the simulation spectra obtained by time-dependent density functional theory (TD-DFT) calculations on a slightly distorted tetrahedral geometry. $\mathbf{1^I}$ and $\mathbf{1^{Br}}$ gradually decomposed to generate the corresponding copper(I) complex and halide radical X•, and in the case of $\mathbf{1^{Br}}$, intramolecular hydroxylation of a methyl group of the TMG substituent took place under aerobic conditions, that may be caused by the reaction of generated copper(I) complex and dioxygen (O_2) generating a reactive oxygen species. $\mathbf{1^X}$ except $\mathbf{1^I}$ showed hydrogen atom abstraction (HAA) reactivity towards cyclohexadiene (CHD), where $\mathbf{1^F}$ exhibited the highest reactivity with a second-order rate constant as 1.4×10^{-3} M^{-1} s^{-1} at 25°C. Such a HAA reactivity can be attributed to the higher basicity of F^- and/or large bond dissociation free energy of conjugate acid H–F as well as unstable copper(II) electronic state in the tetrahedral geometry.

1. INTRODUCTION

Copper(II) complexes favor to take square planar, square pyramidal, or trigonal bipyramidal structure. However, some copper monooxygenases such as peptidylglycine α-hydroxylating monooxygenase (PHM) and dopamine β-monooxygenase (DβM) have a mononuclear tetrahedrally distorted copper reaction center having a labile coordination site for dioxygen binding and activation.[1,2] Thus, it is highly desired to explore the redox reactivity of copper(II) complexes having such an unusual structural feature. In this context, *cis,cis*-1,3,5-triaminocyclohexane (tach) provides an ideal ligand framework that can enforce the metal ion to take a tetrahedral (T_d) geometry with an axial coordination site for the binding of an external substrate.[3-11] However, the strong tendency of copper(II) ion to take the tetragonal basal structures hampers the synthesis of copper(II) complexes taking T_d geometry. Namely, a counter anion and/or solvent molecule easily coordinate to the metal center to break the T_d geometry. Moreover, tetrahedral distortion destabilizes copper(II) complexes through enhancement of electron acceptability. For instance, bis(2,9-dimethyl-1,10-phenanthroline)copper(II) complex taking a T_d geometry is reduced to the corresponding copper(I) complex even by residual water in solvents.[12]

To overcome such difficullties, we employed a bulky and strongly electron donating substituent TMG (*N,N,N′,N′*-tetramethylguanidine) to develop a new tridentate ligand, TMG_3tach ((2,2′,2″-((1s,3s,5s)-cyclohexane-1,3,5-triyl)tris(1,1,3,3-tetramethyl-guanidine)).[13] The TMG substituent has recently been employed in model studies of metallo-oxygenase.[14-21] By using this ligand, we have succeeded to prepare copper(II) complexes taking a tetrahedral geometry with a labile axial coordination site (Scheme 1).[13,22] For instance, copper(II)-bromide complex $\mathbf{1^{Br}}$ can be converted to a methoxide complex $\mathbf{1^{OMe}}$ by the reaction of $\mathbf{1^{Br}}$ with $^nBu_4NOH$ (tetra-*n*-butylammonium hydroxide) in methanol.[13] Moreover, the reaction of $\mathbf{1^{OMe}}$ with C_6F_5OH, C_6F_5SH (C_6F_5 = pentafuluorophenyl; Ar), and an alkylhydroperoxide (ROOH) gave the corresponding phenolate ($\mathbf{1^{OAr}}$), thiophenolate ($\mathbf{1^{SAr}}$), and alkylperoxide copper(II) ($\mathbf{1^{OOR}}$) complexes, respectively (Scheme 1).[13,22] These results clearly demonstrated that the axial coordination site in $\mathbf{1^X}$ is labile to undergo ligand exchange reaction with external substrates.

Scheme 1. Preparation of Tetrahedral Copper(II) Complexes through Axial Ligand Exchange Reactions.

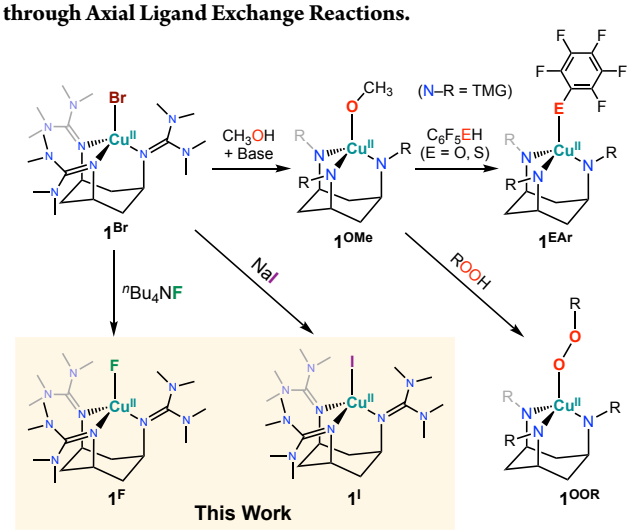

Meanwhile, halide complexes of high-valent group 10 metals such as Ni^{III} and Pd^{IV} have been demonstrated to induce aliphatic C–H bond activation, where homolytic metal–halide bond (M–X) cleavage is proposed to occur to generate halogen radical (X•) as the hydrogen atom accepter from aliphatic substrates.[23-31] Regarding to group 11 metals, however, a little is known about such reactivity of M–X complexes.[32,33] Stieber, Zhang, and coworkers recently reported the aliphatic C–H fluorination using a Cu^{III}–F complex,[34] and McDonald and coworkers reported C–H and O–H bond activation reactivity of a Au^{III}–Cl complex.[35] In this study, we prepared Cu^{II}–F and Cu^{II}–I complexes supported by TMG_3tach ($\mathbf{1^F}$ and $\mathbf{1^I}$), and compared their physicochemical properties and C–H bond activation reactivity with those of $\mathbf{1^{Cl}}$ and $\mathbf{1^{Br}}$ (Scheme 2). As mentioned above, high-valent metal ions (Ni^{III}, Pd^{IV}, Cu^{III}, and Au^{III}) were used to induce the M–X bond cleavage, but we expect that the tetrahedral Cu^{II} complex can also induce such M–X bond cleavage even though Cu^{II} is not a high-valent metal ion, since the tetrahedral geometry is more suited for the lower Cu^{I} oxidation state.

Scheme 2. C–H Bond Activation by $\mathbf{1^X}$

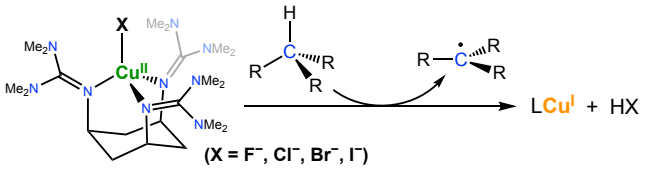

2. RESULTS AND DISCUSSION

2.1. Preparation of Cu^{II}-fluoride ($\mathbf{1^F}$) and Cu^{II}-iodide ($\mathbf{1^I}$) Complexes. We have already reported the synthesis and characterization of Cu^{II}-chloride ($\mathbf{1^{Cl}}$) and Cu^{II}-bromide ($\mathbf{1^{Br}}$) complexes, which can be readily obtained by treating the ligand (TMG_3tach) and $CuCl_2$ and $CuBr_2$, respectively.[13] However, CuF_2 is insoluble in ordinary organic solvents and CuI_2 is not easily available. Thus, we tried to prepare $\mathbf{1^F}$ and $\mathbf{1^I}$ by ligand exchange reaction of the axial bromide ligand of $\mathbf{1^{Br}}$ with fluoride or iodide anion using tetrabutylammonium fluoride ($^nBu_4NF$) and NaI, respectively (Scheme 1).

Ligand exchange reaction of $\mathbf{1^{Br}}$ with 1 equiv of tetrabutylammonium fluoride ($^nBu_4NF$) proceeded quite efficiently to give fluoride complex $\mathbf{1^F}$ in CH_3CN at 25°C, demonstrating stronger Cu^{II}–F bond compared to the Cu^{II}–Br bond. In Figure 1(a) is shown a spectral change observed upon the addition of 1 equiv of $^nBu_4NF$ to $\mathbf{1^{Br}}$ in CH_3CN, where the absorption bands at 410 nm (ε = 1,470 M^{-1} cm^{-1}) and 560 nm (1,080 M^{-1} cm^{-1}) due to $\mathbf{1^{Br}}$ (black) decreased to give new absorption bands at 350 nm (ε = 805 M^{-1} cm^{-1}) and 445 nm (520 M^{-1} cm^{-1}) together with a weak d–d band at 900 nm (100 M^{-1} cm^{-1}) (red). The ESI-MS (positive mode) of the solution showed a major peak cluster at m/z = 505.31, the peak position as well as the isotope distrubution pattern of which were consistent with molecular formula of mononuclear copper(II)-fluoride complex, $[Cu^{II}(TMG_3tach)(F)]^+$ ($\mathbf{1^F}$) (Figure 1(b)).

On the other hand, a large excess of iodide ion was required to reach quantitative formation of the iodide complex $\mathbf{1^I}$, indicating weaker Cu^{II}–I bond compared to the Cu^{II}–Br bond. Treatment of $\mathbf{1^{Br}}$ (0.12 mM) with an excess amount of NaI (500 equiv) in CH_3CN at 25°C resulted in a spectral change to give $\mathbf{1^I}$ exhibiting absorption bands at 470 nm (ε = 1,380 M^{-1} cm^{-1}) and 575 nm (1,660 M^{-1} cm^{-1}) together with a weak and broad absorption band in the near IR region (λ_{max} = 1,140 nm, ε = 200 M^{-1} cm^{-1}) (Figure S1, red). Generated complex $\mathbf{1^I}$, however, gradually decomposed to give Cu^{I} complexes and I_3^- (93 % based on $\mathbf{1^I}$) at 25°C (Figure S1 and S2), indicating that homolytic Cu^{II}–I bond cleavage took place at room temperature. Thus, the reaction of $\mathbf{1^{Br}}$ and NaI was conducted at a lower temperature (–40°C) to stabilize the generated $\mathbf{1^I}$ (Figure S3), and the equilibrium constant of the ligand exchange process was determined to be 0.093 by the titration experiment at –40°C shown in Figure S4. The formation of $\mathbf{1^I}$ was confirmed by ESI-MS, which exhibited a peak cluster at m/z = 613.18, the peak position as well as the isotope distribution pattern were consistent with the chemical formula of $(TMG_3tach)Cu^{II}I$ ($\mathbf{1^I}$) (Figure S5).

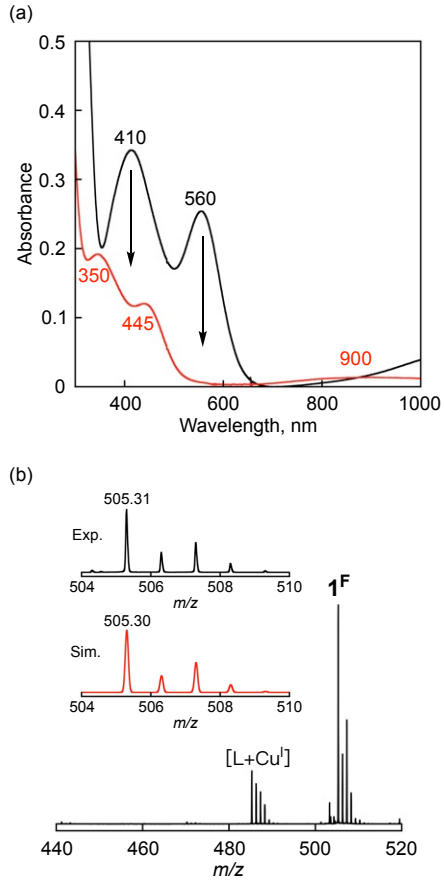

Figure 1. (a) UV-vis spectral change observed upon an addition of $^nBu_4NF$ (1 equiv) to an CH_3CN solution of $\mathbf{1^{Br}}$ (0.25 mM, black) generating $\mathbf{1^F}$ (red) at 25°C. (b) ESI-MS of $\mathbf{1^F}$ in CH_3CN at 25°C. Inset: An expanded spectrum (black) and its simulation spectrum (red).

2.2. Pysicochemical Propeties of Cu^{II}-halide Complexes $\mathbf{1^X}$. EPR spectra of $\mathbf{1^X}$ were measured in acetone (Figure 2 and Figure S6). Although the EPR spectra of $\mathbf{1^{Cl}}$ and $\mathbf{1^{Br}}$ in CH_2Cl_2 have already been reported in our previous paper,[13] those in acetone were re-examined to obtain better hyperfine structures. Simulations of the spectra gave relatively large g_z and small A_z values (Table 2), which are the typical spectral feature of the copper(II) complexes having a tetrahedral geometry.[36,37] It should be noted that $\mathbf{1^F}$ is a rare example of mononuclear copper(II)-fluoride complex having a tetrahedral geometry, even though single crystals suitable for X-ray crystallographic analysis has yet to be obtained despite our great efforts.

Cyclic voltammetric measurements of $\mathbf{1^F}$ gave only a definitive reduction peak at –1.48 V (vs ferrocene/ferrocenium) (Figure S7). This is due to instability of the mononuclear Cu^{I} complex of TMG_3tach as suggested by synthetic difficulty of it.[13] Namely,

treatment of the ligand and $[Cu^{I}(CH_3CN)_4](OTf)$ always provided a trinulcer copper(I) conplex taking a linear two-cordinate geometry at the copper(I) center.[13] In fact, $\mathbf{1^{Cl}}$, $\mathbf{1^{Br}}$, and $\mathbf{1^{I}}$ complexes also showed irreversible voltammograms with reduction peaks at –0.72 V, –0.67 V, and –0.59 V, respectively. Although the accurate redox potentials of $\mathbf{1^{X}}$ could not be determined, the systematic negative shift of the reduction peak potentials in going from iodide to fluoride is consistent with the order of electron donor ability of the halide ligands. For instance, iodide anion has the smallest electron donor ability to the copper center, thus having the smallest impact on the ligand field splitting consistent with the lowest d–d absorption band energy of $\mathbf{1^{I}}$ (see below).

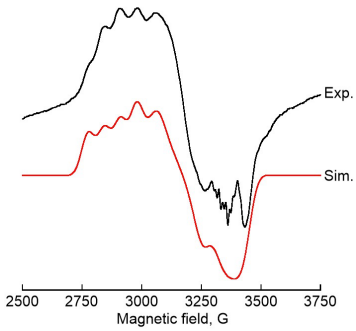

Figure 2. X-band EPR spectrum of $\mathbf{1^{F}}$ (0.5 mM) measured in acetone at 110 K (Exp. black) and its simulation spectrum (Sim. red) generated by using parameters: $g_z = 2.38$, $g_y = 2.17$, $g_x = 2.01$, $A_z = 66$ G, $A_y = 48$ G, $A_x = 32$ G.

2.3. DFT Calculation Studies for Cu^{II}-halide Complexes $\mathbf{1^{X}}$. The electronic structures of $\mathbf{1^{X}}$ were deduced by the DFT calculation performed at the UB3LYP/6-311+G(D) level of theory. Selected bond lengths and angles around the metal centers of optimized structures of $\mathbf{1^{X}}$ are listed in Table 1 together with those of $\mathbf{1^{Cl}}$ and $\mathbf{1^{Br}}$ determined by X-ray crystallographic analysis indicated in parentheses.[13] The bond lengths and angles as well as the τ_4 values[38] in the crystal strucutres of $\mathbf{1^{Cl}}$ and $\mathbf{1^{Br}}$ were well reproduced by the DFT calculation, demonstrating validity of the calculation method. As shown in Figure 3, $\mathbf{1^{F}}$ and $\mathbf{1^{I}}$ take slightly distorted tetrahedral geometry as in the case of $\mathbf{1^{Cl}}$ and $\mathbf{1^{Br}}$. The τ_4 value of the iodide complex was the largest (0.83) among the Cu-halide complexes, and the value decreases with decreasing of the ionic radie of the halide ligand in the order of $\mathbf{1^{I}} > \mathbf{1^{Br}} > \mathbf{1^{Cl}} > \mathbf{1^{F}}$ (Table 1). The major difference appears in the N2–Cu–X angle, which decreses in going from $\mathbf{1^{F}}$ (138.55°) to $\mathbf{1^{Cl}}$ (128.09°) to $\mathbf{1^{Br}}$ (127.11°) and to $\mathbf{1^{I}}$ (125.28°) as shown in Figure 3. The steric repulsion between the bulky TMG substituents on the nitrogen donor atoms and the halide ion decreses in the order of I > Br > Cl > F (Figure S8), allowing the metal center to take more favoralbe tetragonal geometry.

In Figure 4 is shown the electronic absorption spectrum of $\mathbf{1^{F}}$ (black dotted) together with the simulated spectrum obtained by TD-DFT calculation (red), and the spectral and TD-DFT data of other complexes are presented in Figure S9 together with the λ_{max} and ε values summarized in Table 2. Red shift and increase of intensity of the absorption bands are recognized when the metal center has a better tetrahedral geometry. Natural transition orbital (NTO) analyses endorsed the assignment of three absorption bands of each complex.[39] Both the excited particles and the holes corresponding to the lowest energy absorption bands ($\mathbf{1^{F}}$: 900 nm, $\mathbf{1^{Cl}}$: 1100 nm , $\mathbf{1^{Br}}$: 1120 nm, $\mathbf{1^{I}}$: 1140 nm) are mainly localized on copper d-orbitals (Table S1, Figure S10). The differences in the absorption coefficient factors can be ascribed to the involvement of 4p orbital components into the orbitals correspond to the exited particle ($\mathbf{1^{F}}$: 0.01%, $\mathbf{1^{Cl}}$: 1.57%, $\mathbf{1^{Br}}$:1.36%, $\mathbf{1^{I}}$:0.46%), and hole ($\mathbf{1^{F}}$: 3.38%, $\mathbf{1^{Cl}}$: 4.56%, $\mathbf{1^{Br}}$: 4.52%, $\mathbf{1^{I}}$: 4.81%). As for relatively strong absorption bands in 300–600 nm, they are assigned as ligand-to-metal charge transfer (LMCT) bands (Table S2, Figures S11 and S12). Both absorption bands are ascribed to the CT from guanidine-moiety to the copper centerr in $\mathbf{1^{F}}$. The higher energy absorption bands involve partial CT from the halide to copper (XMCT) in $\mathbf{1^{Cl}}$ (30%) and $\mathbf{1^{Br}}$ (60%), and the lower energy bands are the LMCT with guanidine based orbitals. The most donating iodide ligand makes the lower energy band (575 nm) to a CT band from iodide (99%) to copper, and the higher energy band (470 nm) is a ligand based CT.

Table 1. Bond Lengths (Å), Bond Angles (deg), and τ_4 Values of the Optimized Structures of $\mathbf{1^{X}}$ Obtained by DFT Calculations at the UB3LYP/6-311+G(D) Level of Theory.

	$\mathbf{1^{F}}$	$\mathbf{1^{Cl}}$	$\mathbf{1^{Br}}$	$\mathbf{1^{I}}$
Cu–X	1.828	2.262 (2.259)	2.378 (2.397)	2.685
Cu–N1	2.000	1.986 (1.953)	1.987 (1.948)	1.978
Cu–N2	1.956	1.947 (1.948)	1.952 (1.945)	1.947
Cu–N3	2.070	2.052 (2.068)	2.061 (2.047)	2.030
N1–Cu–X	107.86	114.13 (114.89)	115.14 (115.56)	114.33
N2–Cu–X	138.55	128.09 (129.80)	127.11 (128.28)	125.28
N3–Cu–X	112.95	117.29 (117.01)	117.92 (116.95)	117.64
τ_4	0.77	0.81 (0.80)	0.82 (0.81)	0.83

Bond lengths, bond angles, and τ_4 values obtained from the crystal structures of $\mathbf{1^{Cl}}$ and $\mathbf{1^{Br}}$ are shown in the parentheses.[13]

Table 2. Electronic Absorption Spectral Data and EPR Parameter of $\mathbf{1^{X}}$

Complex	λ/nm (ε/M^{-1} cm^{-1})			g_x, g_y, g_z (g_{iso})	A_x, A_y, A_z/G
$\mathbf{1^{F}}$	340 (930)	445 (620)	800 (70)	2.01, 2.17, 2.38 (2.19)	32, 48, 66
$\mathbf{1^{Cl}}$	405 (1,030)	535 (1,360)	1100 (210)	2.00, 2.11, 2.32 (2.14)	58, 33, 65
$\mathbf{1^{Br}}$	410 (1,395)	560 (1,075)	1120 (220)	2.00, 2.11, 2.32 (2.14)	61, 44, 31
$\mathbf{1^{I}}$	470 (1,200)	575 (1,420)	1140 (220)	2.04, 2.05, 2.32 (2.14)	62, 80, 18

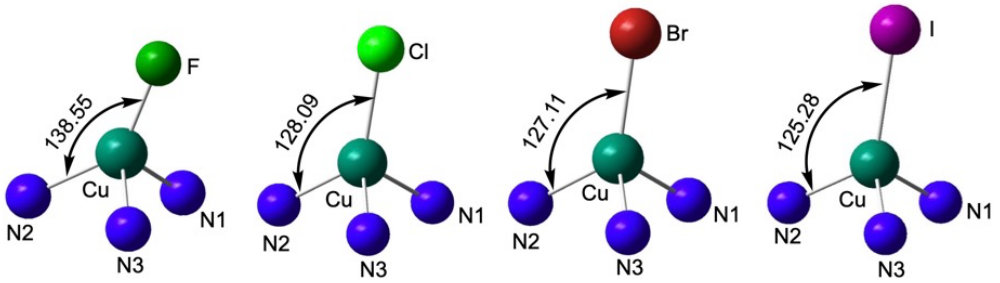

Figure 3. Cu centers of the optimized structures of $\mathbf{1^X}$ by DFT calculations with UB3LYP/6-311+G(D) basis set.

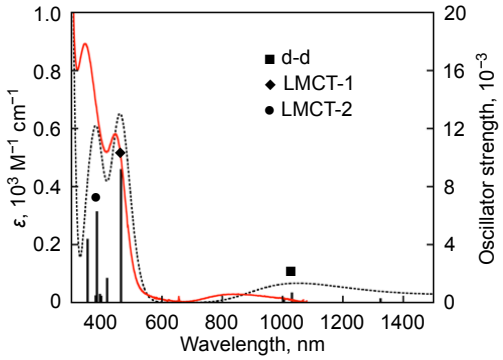

Figure 4. UV-vis-NIR spectrum of 1^F in CH_3CN measured at 25°C (red) and the calculated electronic absorption bands (bar) and a corresponding spectrum (black dotted line, peak half-width at half height is 0.2 eV).

2.4. Self-decomposition Cu^{II}-halide Complexes $\mathbf{1^X}$. As described above, $\mathbf{1^I}$ gradually decomposed to give the copper(I) complex and I_3^- (93% based on $\mathbf{1^I}$), indicating that homolytic Cu^{II}–I bond cleavage took place. $\mathbf{1^{Br}}$ also underwent self-decomposition to give the copper(I) complex under anaerobic conditions, but its stability ($t_{1/2} = 5 \times 10^3$ sec at 70°C in CH_3CN, see Figure S13) was higher than that of $\mathbf{1^I}$ ($t_{1/2} = 7.9 \times 10^2$ sec at 25°C in CH_3CN, see Figure S1). When the self-decomposition of $\mathbf{1^{Br}}$ was carried out under O_2 atmosphere, ligand hydroxylation reaction took place to give a green solid in about 50% yield. X-ray crystallographic analysis of the sample revealed that the product was a trinuclear copper(II) complex **2,** which consists of two molecules of copper(II) complex of a hydroxylated ligand that are connected by a copper(II) ion (Cu1) through hydroxide (O1 and O1') and alkoxide (O2 and O2') bridges (Figure S14). The copper(II) ions (Cu2 and Cu2') ligated by the hydroxylated ligand exhibit a distorted square pyramidal geometry with three nitrogen atoms (N1, N4, N7 and N1', N4', N7') of the ligand and two oxygen atoms of the hydroxide (O1 and O1') and alkoxide (O2 and O2') groups, and the bridging copper(II) ion (Cu1) exhibits square planer geometry with the four oxygen atoms (O1, O1', O2, and O2').

The ligand hydroxylation at one of the TMG substituents was further confirmed by ESI-MS of the post-reaction solution (Figure S15) and ^{1}H NMR of the organic compounds obtained after ordinary demetalation treatment using aquaous anmonia (see Experimental Section, Figure S16). In the ESI-MS, peak clusters assignable to the copper(II) complexes of hydroxylated ligand were observed at 501,30, 529.30, and 546,29, the peak positions and isotope distribution patterns were consisten with the molecular formulas of $[Cu^{II}(L\text{-}O)]^+$, $[Cu^{II}(L\text{-}O)(N_2)]^+$, $[Cu^{II}(L\text{-}O)(CO_2)]^+$, respectively (L-O is deprotonated hydroxylated ligand. The N_2 and CO_2 complexes may be generated during the MS measurement in the equipment). There was also a peak cluster at 486.31, which was assignable to the copper complex of a demethylated ligand (L – CH_3) generated by oxidative demethylation. In the ^{1}H NMR spectrum (Figure S16), the methylene protons of the –CH_2OH group of hydroxylated ligand (L-OH) was observed at $\delta = 5.29$, but its integration ratio was smaller than expected value (two protons). This is due to oxidative demethylation of the ligand as demonstrated by the ESI-MS data (peak cluster at 486.31 in Figure S15).

Mechanistic details of the ligand hydroxylation reaction are not clear since the reaction was too slow to perform detailed mechanistic study. Nonetheless, it can be assumed that homolytic cleavage of the Cu^{II}–Br bond generates a Cu^I complex and Br•, the former of which may react with O_2 to generate a Cu^{II}-active oxygen speceis $\mathbf{1^{O_2}}$ to trigger the aliphatic ligand hydroxylation reaction (Scheme 3).[40,41] On the other hand, generated Br• dimerizes to give Br_2, which volatiles during the reaction at the higher temperature (70°C). In this reacion, isolated sample of $\mathbf{1^{Br}}$ was used, so that there was no extra Br^- to trap Br_2 in the solution. The same ligand hydroxylation product was obtained by treating the isolated copper(I) complex of TMG_3tach ligand under O_2 atmosphere, demonstrating accuracy of the proposed mechanism (Scheme 3). Notably, $\mathbf{1^{Cl}}$ and $\mathbf{1^F}$ were stable at 70°C, indicating stronger Cu^{II}–Cl and Cu^{II}–F bonds compared to the Cu^{II}–I and Cu^{II}–Br bonds.

Scheme 3. Presumed Ligand Hydroxylation Pathway from $\mathbf{1^{Br}}$

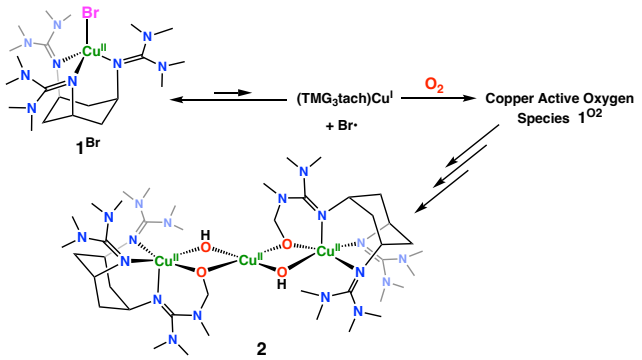

2.4. C–H Bond Activation of External Substrate. C–H bond activation reactivity of $\mathbf{1^X}$ was then examined by using 1,4-cyclohexadiene (CHD) as an external substrate. A typical example of the spectral change for the reaction of $\mathbf{1^F}$ and CHD is shown in Figure 5(a). Addition of an excess amount of CHD to a CH_3CN solution of $\mathbf{1^F}$ (0.25 mM) at 25°C resulted in quantitative formation of

benzene based on $\mathbf{1^F}$, which was confirmed by FID-GC using a calibration curve. Generation of HF was also confirmed by ^{19}F-NMR of the post reaction solution (Figure S17), whereas ligand fluorination reaction was not observed. The reaction obeyed first-order kinetics, and the pseudo-first-order rate constant (k_{obs}) was determined from the linear plot of $\ln(A - A_\infty)$ vs. reaction time based on the absorption change at 445 nm (Figure 5(a), inset). The second-order rate constant (k) was then determined as 1.4×10^{-3} M^{-1} s^{-1} from the slope of the linear dependence of k_{obs} against the concentration of CHD (Figure 5(b)). Notably, this is the first example of hydrogen abstraction reaction by a copper(II)-fluoride complex. $\mathbf{1^{Cl}}$ and $\mathbf{1^{Br}}$ could also oxidize CHD, but their reaction rates were much smaller than that of $\mathbf{1^F}$ as shown in Figures S18 and S19, respectively. Since these reactions were too slow to perform detailed kinetic analysis, the reaction rates were roughly estimated using their half-life times; 7.0×10^3 sec and 2.5×10^4 sec, respectively. On the other hand, iodide complex $\mathbf{1^I}$ hardly reacted with CHD under the same reaction conditions. Thus, the reactivity of the halide complexes toward CHD increases in the order of $\mathbf{1^I} << \mathbf{1^{Br}} < \mathbf{1^{Cl}} < \mathbf{1^F}$. This trend seems to correlate with the order of pK_b values of X^- and/or bond dissociate free energy (BDFE) of the conjugate acid H–X, but not the electron transfer reactivity of $\mathbf{1^X}$ as shown in Table S4.[42,43]

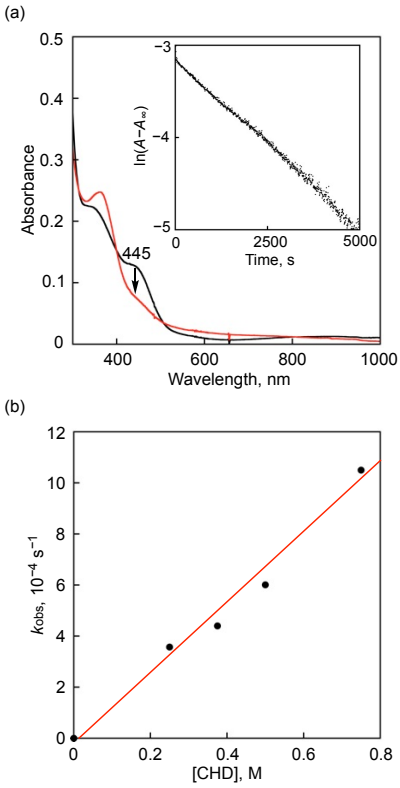

Figure 5. (a) UV-vis spectral change for the reaction of $\mathbf{1^F}$ (0.25 mM) with 1,4-cyclohexadiene (CHD, 250 mM) in CH_3CN at 25°C. Inset: first-order plot based on the absorption change at 445 nm. (b) Plot of k_{obs} vs. [CHD] for the reaction of $\mathbf{1^F}$ with 1,4-cyclohexadiene (CHD).

The reactivity tendency is the same to that of the high-valent Cu^{III}–X system showing hydrogen atom abstracting (HAA) reactivity toward 9,10-dihydroanthracene reported by Zhang and co-workers.[34] Similarly, MacDonald reported a high-valent Ni^{III}–F complex showing a higher HAA reactivity than that of corresponding Ni^{III}–Cl complex.[29] Such a high HAA reactivity of the trivalent metal–halide complexes are attributed to the proton and electron acceptability of the halide ligand and the metal center, respectively. Thus, we think that $\mathbf{1^X}$ may abstract hydrogen atom from the substrate via a similar mechanism, where the high HAA ability of $\mathbf{1^F}$ is created by the high pK_b values of F^- and/or the high bond dissociate free energy (BDFE) of the conjugate acid H–F as well as the unstable tetrahedral structure of the copper(II) oxidation state. Unfortunately, relatively low reactivity of $\mathbf{1^X}$ hampered us to perform detailed systematic studies such as correlation between the reaction rate and BDFE of the series of substrates and kinetic isotope effect using deuterated substrate.

3. CONCLUSION

In this study, we have evaluated the strucutres, physicochemical properties, and C–H bond activation reactivity of the whole series of copper(II)-halide complexes $\mathbf{1^X}$ supported by TMG_3tach ligand, which enforces the copper(II) center to take an unusual tetrahedral geometry with a labile axial coordination site. Disorder of the geometry from the ideal tetrahedral one increases as the ionic size of the halide ligand decreased as $\mathbf{1^I} > \mathbf{1^{Cl}} > \mathbf{1^F} > \mathbf{1^I}$. Such a geometric effect imperts the compressed ligand field splitting of the copper center and larger participation of copper 4p orbital into the electronic absorption, thus alternating the λ_{max} and ε values of the d–d bands. Strength of the Cu^{II}–X bond increases in the order of I < Br < Cl < F to enhance the stability of the copper(II) complexes. Thus, the less stable $\mathbf{1^I}$ and $\mathbf{1^{Br}}$ easily underwent Cu^{II}–X bond homolysis to generate Cu^I complex and $X^\bullet$. The generated Cu^I complex reacted with O_2 to induce aliphatic ligand hydroxylation reaction through the formation of a Cu^{II}-active oxygen complex. On the other hand, $\mathbf{1^F}$ induced direct C–H bond activation of the external substrate CHD. Such a reacitvity can be attributed to the high pK_b values of F^- and/or the high bond dissociate free energy (BDFE) of the conjugate acid H–F as well as the unstable tetrahedral structure of the copper(II) oxidation state.

4. EXPERIMENTAL SECTION

4.1. General. The reagents and solvents used in this study, except the ligand and the copper complexes, were commercial products of the highest available purity and used as received without further purification,[44] unless otherwise noted. Ligand, TMG_3tach, and its Cu(II) complexes, $\mathbf{1^{Cl}}$ and $\mathbf{1^{Br}}$, were prepared according to the reported procedures.[13] All reactions were carried out under N_2 atmosphere using standard Schlenkline or a gloveboxes (miwa DB0-1KP or KK-011-AS, KOREA KIYON product, [O_2]<1 ppm). UV-visible spectra were taken on a Jasco V-570 or a Hawlett Packard 8453 photo diode array spectrophotometer equipped with a Unisoku thermostated cryostat cell holder USP-203. ^{1}H-NMR spectra were recorded on a JEOL JNM-ECS400 or a JEOL ECS400 spectrometer. Electrospray ionization mass spectra (ESI-MS) measurements were performed on a microTOF II focus (Bruker Daltonics). Electron paramagnetic resonance (EPR) spectra were measured on a BRUKER EMX-micro continuous-wave X-band spectrometer, and simulated with the SpinCount program.[45] Electrochemical measurements (cyclic voltammetry) were performed at 298 K using an Automatic Polarization System HZ-7000 in deaerated acetonitrile (CH_3CN) containing ^{n}Bu$_4$NPF$_6$ (tetra-*n*-butylammonium hexafluorophosphate, 0.10 mM) as a supporting electrolyte. A conventional three-electrode cell was used with a glassy carbon working electrode and a platinum wire as a counter electrode. The measured potentials were recorded with respect to Ag/$AgNO_3$ (1.0×10^{-2} M). All electrochemical measurements of the copper complexes were carried out under a nitrogen atmosphere. All redox potentials are referenced to ferrocene/ferrocenium (Fc/Fc^+) redox potential.

4.2. Generation of $\mathbf{1^F}$. An acetonitrile solution (50 μL) of ^{n}Bu$_4$NF (15 mM) was added to an acetonitrile solution (3.0 mL) of $\mathbf{1^{Br}}$ (0.25

mM) in a UV cell (1.0 cm path length) at 25 °C to generate $\mathbf{1^F}$ immediately. UV-vis (CH_3CN, 25 °C): λ_{max} = 350 nm (ε = 805 M^{-1} cm^{-1}), 445 nm (ε = 520 M^{-1} cm^{-1}), and 900 nm (ε = 100 M^{-1} cm^{-1}); ESI-MS (positive mode): m/z = 505.31, calcd for $[Cu^{II}(TMG_3tach)F]^+$ ($C_{21}H_{45}CuFN_9$), 505.30.

4.3. Generation of $\mathbf{1^I}$. An acetonitrile solution (150 μL) of NaI (1200 mM) was added to an acetonitrile solution (3.0 mL) of $\mathbf{1^{Br}}$ (0.12 mM) in a UV cell (1.0 cm path length) at −40 °C to generate $\mathbf{1^I}$ immediately. UV-vis (CH_3CN, −40 °C): λ_{max} = 470 nm (ε = 1380 M^{-1} cm^{-1}), 575 nm (ε = 1660 M^{-1} cm^{-1}), and 1140 nm (ε = 200 M^{-1} cm^{-1}); ESI-MS (positive mode): m/z = 613.18, calcd for $[Cu^{II}(TMG_3tach)I]^+$ ($C_{21}H_{45}CuIN_9$), 613.21.

4.4. Preparation of 2. $[Cu^{II}(TMG_3tach)Br]ClO_4$ (5.0 mg, 7.0 μmol) dissolved in CH_3CN (1.0 mL) was stirred at 70°C under O_2 atmosphere for 18 h. Then, reaction mixture was filtered to remove insoluble material, and the filtrate was concentrated under reduced pressure to obtain a green solid (1.6 mg, 50 %). Single crystals suitable for X ray crystallographic analysis were obtained by recrystallization from THF/hexane (Table S3 and Figure S14). The hydroxylated ligand was recovered as a mixture of the original ligand by the ordinary demetallation treatment. Thus, the post-reaction solution was treated with 5.0 mL of 28 % aqueous ammonia solution, and then extracted by CH_2Cl_2 (5 mL x 3). The combined organic layer was dried over $MgSO_4$ and concentrated under reduced pressure after removal of $MgSO_4$ by filtration. ^{1}H NMR spectrum of the organic compounds is shown in Figure S16; ^{1}H NMR (400 MHz, $CDCl_3$) δ = 5.29 (s, −C<u>H$_2$</u>OH).

4.5. X-ray Structure Determination. All single crystals obtained in this study were mounted on a DT-MicroLoop (MiTegen, LLC) with mineral oil, and all X-ray date were collected at −163°C on a Rigaku R-AXIS RAPID diffractometer using filtered Mo-*Kα* radiation. The structures were solved by direct method (SIR2011) and expanded using Fourier techniques.[46] Non-hydrogen atoms were refined anisotropically by full-matrix least squares on F^2. Hydrogen atoms were attached at idealized positions on carbon atoms and were not refined. All structures in the final stages of refinement showed no movement in the atom positions. The calculations were performed using Single-Crystal Structure Analysis Software, version 4.1 (Rigaku Corporation: The Woodlands, TX). The crystallographic data of **2** are summarized in Table S3 and the selected bond lenghths and angles are presented in the figure caption of Figure S14.

4.6. Theoretical Calculations. DFT calculations were performed by using Gaussian 09 (revision D.01; Gaussian, Inc.).[47] Molecular structures were optimized by using the UB3LYP functional with 6-311+G(d) basis set. For the optimized geometry, normal coordinate analyses for energy minima were performed to confirm no imaginary frequency. Electronic excitation energies and intensities were computed by the time-dependent TD-DFT calculations at the same level to its geometric optimization.[48] The first 30 excited states were calculated. Graphical outputs of the computational results were generated with the GaussView software program (ver. 5.0.8) developed by Semichem, Inc.[49]

4.7. Kinetic Measurements. Kinetic measurements for the reaction of copper(II) halide complexes $\mathbf{1^X}$ with external substrates were performed using a Hawlett Pckard 8453 photo diode array spectrophotometer equipped with a Unisoku thermostaic cryostat cell holder USP-203 (a desired temperature can be fixed within ± 0.5°C) in CH_3CN. Typically, after formation of $\mathbf{1^F}$ by the reaction of $\mathbf{1^{Br}}$ (0.25 mM) with an equimolar amount of ^{n}Bu$_4$NF·3H$_2$O at 0–25°C in CH_3CN, the reactions were initiated by injecting a substrate solution into the solution of $\mathbf{1^F}$ with use of a microsyringe at a desired temperature. The amount of the added substrates is kept more than 2.5 mM to maintain the pseudo-first-order-reaction conditions. The reactions were monitored by following decrease in absorbance at 445 nm, and the pseudo-first-order-rate constants (k_{obs}) of the reactions were obtained from the plot of ln(ΔA) aginst time (t).

ASSOCIATED CONTENT

Supporting Information

The Supporting Information is available free of charge on the ACS Publications website.

Experimental data including DFT calculation results, X-ray crystallographic analysis data, spectral data (UV-vis-NIR, ESI-MS, EPR), cyclic voltammograms, and kinetic analysis data.

Accession Code

CCDC-2238502 contains the supplementary crystallographic data for this paper. These data can be obtained free of charge via www.ccdc.cam.ac.uk/data_request/cif, or by emailing data_request@ccdc.cam.ac.uk, or by contacting The Cambridge Crystallographic Data Centre, 12 Union Road, Cambridge CB2 1EZ, UK; fax: +44 122 336033.

AUTHOR INFORMATION

Corresponding Author

Shinobu Itoh – *Department of Molecular Chemistry, Division of Applied Chemistry, Graduate School of Engineering, Osaka University, 2-1 Yamada-oka, Suita, Osaka 565-0871, Japan;* orcid.org/0000-0002-3711-2378; Email: shinobu@chem.eng.osaka-u.ac.jp

Authors

Yang Lan – *Department of Molecular Chemistry, Division of Applied Chemistry, Graduate School of Engineering, Osaka University, 2-1 Yamada-oka, Suita, Osaka 565-0871, Japan*

Yuma Morimoto – *Department of Molecular Chemistry, Division of Applied Chemistry, Graduate School of Engineering, Osaka University, 2-1 Yamada-oka, Suita, Osaka 565-0871, Japan;* orcid.org/0000-0002-5209-266X

Ikuma Shimizu – *Department of Molecular Chemistry, Division of Applied Chemistry, Graduate School of Engineering, Osaka University, 2-1 Yamada-oka, Suita, Osaka 565-0871, Japan*

Hideki Sugimoto – *Department of Molecular Chemistry, Division of Applied Chemistry, Graduate School of Engineering, Osaka University, 2-1 Yamada-oka, Suita, Osaka 565-0871, Japan;* orcid.org/0000-0002-4887-1740.

Funding Sources

This work was supported by JST-CREST (JPMJCR16P1 to SI) and JST SPRING (Grant Number JPMJSP2138 to YL).

Notes

The authors declare no competing financial interest.

REFERENCE

(1) Prigge, S. T.; Eipper, B. A.; Mains, R. E.; Amzel, L. M. Dioxygen Binds End-on to Mononuclear Copper in a Precatalytic Enzyme Complex. *Science* **2004,** 304 (5672), 864-867.

(2) Solomon, E. I.; Heppner, D. E.; Johnston, E. M.; Ginsbach, J. W.; Cirera, J.; Qayyum, M.; Kieber-Emmons, M. T.; Kjaergaard, C. H.; Hadt, R. G.; Tian, L. Copper Active Sites in Biology. *Chem. Rev.* **2014,** 114 (7), 3659-3853.

(3) Cronin, L.; Greener, B.; Foxon, S. P.; Heath, S. L.; Walton, P. H. Syntheses and Single-crystal X-ray Structures of a Series of Monosubstituted *cis,cis*-1,3,5-Triaminocyclohexane-based Complexes. *Inorg. Chem.* **1997,** 36 (12), 2594-2600.

(4) Cronin, L.; Walton, P. H. Synthesis and Structure of $[Zn(OMe)(L)]\cdot[Zn(OH)(L)]_2\cdot(BPh_4)$, L = *cis,cis*-1,3,5-tris[(*E,E*)-3-(2-furyl)acrylideneamino]cyclohexane: Structural Models of Carbonic Anhydrase and Liver Alcohol Dehydrogenase. *Chem. Commun.* **2003,** (13), 1572-1573.

(5) Nairn, A. K.; Archibald, S. J.; Bhalla, R.; Boxwell, C. J.; Whitwood, A. C.; Walton, P. H. Syntheses of Copper(I) *cis*-1,3,5-Tri-iminocyclohexane Complexes. *Dalton Trans.* **2006,** (14), 1790-1795.

(6) Kajita, Y.; Arii, H.; Saito, T.; Saito, Y.; Nagatomo, S.; Kitagawa, T.; Funahashi, Y.; Ozawa, T.; Masuda, H. Syntheses, Characterization, and Dioxygen Reactivities of Cu(I) Complexes with *cis*,*cis*-1,3,5-Triaminocyclohexane Derivatives: A $Cu(III)_2O_2$ Intermediate Exhibiting Higher C–H Activation. *Inorg. Chem.* **2007,** 46 (8), 3322-3335.

(7) Cushion, M.; Ebrahimpour, P.; Haddow, M. F.; Hallett, A. J.; Mansell, S. M.; Orpen, A. G.; Wass, D. F. Copper(I) Complexes of *cis*,*cis*-1,3,5-Tris(mesitylideneamino)cyclohexane Ligands: Synthesis, Structure and Substrate Selectivity. *Dalton Trans.* **2009,** (9), 1632-1635.

(8) Ebrahimpour, P.; Cushion, M.; Haddow, M. F.; Hallett, A. J.; Wass, D. F. Cu(I) Complexes Based on *cis*,*cis*-1,3,5-Tris(arylideneamino)cyclohexane Ligands: Synthesis, Structure and CO Binding. *Dalton Trans.* **2010,** 39 (45), 10910-10919.

(9) Rocks, S. S.; Brennessel, W. W.; Machonkin, T. E.; Holland, P. L. Solution and Structural Characterization of Iron(II) Complexes with *ortho*-Halogenated Phenolates: Insights Into Potential Substrate Binding Modes in Hydroquinone Dioxygenases. *Inorg. Chem.* **2010,** 49 (23), 10914-10929.

(10) Matsumoto, J.; Kajita, Y.; Masuda, H. Synthesis and Characterization of a (μ-η^2:η^2-Peroxido)dicopper(II) Complex with *N*,*N'*,*N''*-Triisopropyl-*cis*,*cis*-1,3,5-triaminocyclohexane (R_3TACH, R = ^{i}Pr): Selective Preparation of (μ-η^2:η^2-Peroxido)dicopper(II) and Bis(μ-oxido)dicopper(III) Species Regulated by Substituent Groups. *Eur. J. Inorg. Chem.* **2012,** 2012 (26), 4149-4158.

(11) Ebrahimpour, P.; Haddow, M. F.; Wass, D. F. New Cu(I)-Ethylene Complexes Based on Tridentate Imine Ligands: Synthesis and Structure. *Inorg. Chem.* **2013,** 52 (7), 3765-3771.

(12) Itoh, S.; Kishikawa, N.; Suzuki, T.; Takagi, H. D. Syntheses, Structural Analyses and Redox Kinetics of Four-coordinate $[CuL_2]^{2+}$ and Five-coordinate $[CuL_2(solvent)]^{2+}$ Complexes (L = 6,6'-Dimethyl-2,2'-bipyridine or 2,9-Dimethyl-1,10-phenanthroline): Completely Gated Reduction Reaction of $[Cu(dmp)_2]^{2+}$ in Nitromethane. *Dalton Trans.* **2005,** (6), 1066-1078.

(13) Shimizu, I.; Morimoto, Y.; Faltermeier, D.; Kerscher, M.; Paria, S.; Abe, T.; Sugimoto, H.; Fujieda, N.; Asano, K.; Suzuki, T.; Comba, P.; Itoh, S. Tetrahedral Copper(II) Complexes with a Labile Coordination Site Supported by a Tris-tetramethylguanidinato Ligand. *Inorg. Chem.* **2017,** 56 (16), 9634-9645.

(14) Schatz, M.; Raab, V.; Foxon, S. P.; Brehm, G.; Schneider, S.; Reiher, M.; Holthausen, M. C.; Sundermeyer, J.; Schindler, S. Combined Spectroscopic and Theoretical Evidence for a Persistent End-on Copper Superoxo Complex. *Angew. Chem., Int. Ed.* **2004,** 43 (33), 4360-4363.

(15) Herres-Pawlis, S.; Florke, U.; Henkel, G. Tuning of Copper(I)-dioxygen Reactivity by Bis(guanidine) Ligands. *Eur. J. Inorg. Chem.* **2005,** (19), 3815-3824.

(16) Würtele, C.; Gaoutchenova, E.; Harms, K.; Holthausen, M. C.; Sundermeyer, J.; Schindler, S. Crystallographic Characterization of a Synthetic 1:1 End-on Copper Dioxygen Adduct Complex. *Angew. Chem., Int. Ed.* **2006,** 45 (23), 3867-3869.

(17) England, J.; Martinho, M.; Farquhar, E. R.; Frisch, J. R.; Bominaar, E. L.; Münck, E.; Que, L. A Synthetic High-Spin Oxoiron(IV) Complex: Generation, Spectroscopic Characterization, and Reactivity. *Angew. Chem., Int. Ed.* **2009,** 48 (20), 3622-3626.

(18) Herres-Pawlis, S.; Verma, P.; Haase, R.; Kang, P.; Lyons, C. T.; Wasinger, E. C.; Florke, U.; Henkel, G.; Stack, T. D. P. Phenolate Hydroxylation in a Bis(μ-oxo)dicopper(III) Complex: Lessons From the Guanidine/Amine Series. *J. Am. Chem. Soc.* **2009,** 131 (3), 1154-1169.

(19) England, J.; Guo, Y.; Van Heuvelen, K. M.; Cranswick, M. A.; Rohde, G. T.; Bominaar, E. L.; Münck, E.; Que, L. A More Reactive Trigonal-Bipyramidal High-spin Oxoiron(IV) Complex with a *cis*-Labile Site. *J. Am. Chem. Soc.* **2011,** 133 (31), 11880-11883.

(20) Pfaff, F. F.; Heims, F.; Kundu, S.; Mebs, S.; Ray, K. Spectroscopic Capture and Reactivity of $S = 1/2$ Nickel(III)-Oxygen Intermediates in the Reaction of a Ni^{II}-salt with *m*-CPBA. *Chem. Commun.* **2012,** 48 (31), 3730-3732.

(21) Peterson, R. L.; Ginsbach, J. W.; Cowley, R. E.; Qayyum, M. F.; Himes, R. A.; Siegler, M. A.; Moore, C. D.; Hedman, B.; Hodgson, K. O.; Fukuzumi, S.; Solomon, E. I.; Karlin, K. D. Stepwise Protonation and Electron-Transfer Reduction of a Primary Copper-Dioxygen Adduct. *J. Am. Chem. Soc.* **2013,** 135 (44), 16454-16467.

(22) Shimizu, I.; Morimoto, Y.; Velmurugan, G.; Gupta, T.; Paria, S.; Ohta, T.; Sugimoto, H.; Ogura, T.; Comba, P.; Itoh, S. Characterization and Reactivity of a Tetrahedral Copper(II) Alkylperoxido Complex. *Chem.–Eur. J.* **2019,** 25 (25), 11157-11165.

(23) Pérez-Temprano, M. H.; Racowski, J. M.; Kampf, J. W.; Sanford, M. S. Competition between sp^3-C–N vs sp^3-C–F Reductive Elimination from Pd^{IV} Complexes. *J. Am. Chem. Soc.* **2014,** 136 (11), 4097-4100.

(24) Hwang, S. J.; Powers, D. C.; Maher, A. G.; Anderson, B. L.; Hadt, R. G.; Zheng, S.-L.; Chen, Y.-S.; Nocera, D. G. Trap-Free Halogen Photoelimination from Mononuclear Ni(III) Complexes. *J. Am. Chem. Soc.* **2015,** 137 (20), 6472-6475.

(25) Hwang, S. J.; Anderson, B. L.; Powers, D. C.; Maher, A. G.; Hadt, R. G.; Nocera, D. G. Halogen Photoelimination from Monomeric Nickel(III) Complexes Enabled by the Secondary Coordination Sphere. *Organometallics* **2015,** 34 (19), 4766-4774.

(26) Shields, B. J.; Doyle, A. G. Direct C(sp^3)–H Cross Coupling Enabled by Catalytic Generation of Chlorine Radicals. *J. Am. Chem. Soc.* **2016,** 138 (39), 12719-12722.

(27) Mondal, P.; Pirovano, P.; Das, A.; Farquhar, E. R.; McDonald, A. R. Hydrogen Atom Transfer by a High-valent Nickel-chloride Complex. *J. Am. Chem. Soc.* **2018,** 140 (5), 1834-1841.

(28) Mondal, P.; Lovisari, M.; Twamley, B.; McDonald, A. R. Fast Hydrocarbon Oxidation by a High-valent Nickel-fluoride Complex. *Angew. Chem., Int. Ed.* **2020,** 59 (31), 13044-13050.

(29) Mondal, P.; McDonald, A. R. Phenol Oxidation by a Nickel(III)–Fluoride Complex: Exploring the Influence of the Proton Accepting Ligand in PCET Oxidation. *Chem.–Eur. J.* **2020,** 26 (44), 10083-10089.

(30) Gygi, D.; Gonzalez, M. I.; Hwang, S. J.; Xia, K. T.; Qin, Y.; Johnson, E. J.; Gygi, F.; Chen, Y.-S.; Nocera, D. G. Capturing the Complete Reaction Profile of a C–H Bond Activation. *J. Am. Chem. Soc.* **2021,** 143 (16), 6060-6064.

(31) Kariofillis, S. K.; Doyle, A. G. Synthetic and Mechanistic Implications of Chlorine Photoelimination in Nickel/Photoredox C(sp^3)–H Cross-Coupling. *Acc. Chem. Res.* **2021,** 54 (4), 988-1000.

(32) Kochi, J. K. The Reduction of Cupric Chloride by Carbonyl Compounds. *J. Am. Chem. Soc.* **1955,** 77 (20), 5274-5278.

(33) Castro, C. E.; Gaughan, E. J.; Owsley, D. C. Cupric Halide Halogenations. *J. Org. Chem.* **1965,** 30 (2), 587-592.

(34) Bower, J. K.; Cypcar, A. D.; Henriquez, B.; Stieber, S. C. E.; Zhang, S. C(sp^3)–H Fluorination with a Copper(II)/(III) Redox Couple. *J. Am. Chem. Soc.* **2020,** 142 (18), 8514-8521.

(35) Lovisari, M.; Gericke, R.; Twamley, B.; McDonald, A. R. Comparing Metal–Halide and –Oxygen Adducts in Oxidative C/O–H Activation: Au^{III}–Cl versus Au^{III}–OH. *Inorg. Chem.* **2021,** 60 (20), 15610-15616.

(36) Sakaguchi, U.; Addison, A. W. Spectroscopic and Redox Studies of Some Copper(II) Complexes with Biomimetic Donor Atoms – Implications For Protein Copper Centers. *J. Chem. Soc., Dalton Trans.* **1979,** (4), 600-608.

(37) Yokoi, H.; Addison, A. W. Spectroscopic and Redox Properties of Pseudotetrahedral Copper(II) Complexes. Their Eelation to Copper Proteins. *Inorg. Chem.* **1977,** 16 (6), 1341-1349.

(38) Yang, L.; Powell, D. R.; Houser, R. P. Structural Variation in Copper(I) Complexes with Pyridylmethylamide Ligands: Structural Analysis with a New Four-coordinate Geometry Index, τ_4. *Dalton Trans.* **2007,** (9), 955-964.

(39) Martin, R. L. Natural Transition Orbitals. *J. Chem. Phys.* **2003,** 118 (11), 4775-4777.

(40) Kunishita, A.; Kubo, M.; Sugimoto, H.; Ogura, T.; Sato, K.; Takui, T.; Itoh, S. Mononuclear Copper(II)-superoxo Complexes that Mimic the Structure and Reactivity of the Active Centers of PHM and DβM. *J. Am. Chem. Soc.* **2009,** 131 (8), 2788-2789.

(41) Kunishita, A.; Ertem, M. Z.; Okubo, Y.; Tano, T.; Sugimoto, H.; Ohkubo, K.; Fujieda, N.; Fukuzumi, S.; Cramer, C. J.; Itoh, S. Active Site Models for the CuA Site of Peptidylglycine α-Hydroxylating Monooxygenase and Dopamine β-Monooxygenase. *Inorg. Chem.* **2012,** 51 (17), 9465-9480.

(42) Bordwell, F. G. Equilibrium Acidities in Dimethyl Sulfoxide Solution. *Acc. Chem. Res.* **1988,** 21 (12), 456-463.

(43) Luo, Y.-R. *Comprehensive Handbook of Chemical Bond Energies*. CRC Press: Boca Raton, FL, 2007.

(44) Armarego, W. L. F. *Purification of Laboratory Chemicals*. Elsevier Science: 2017.

(45) Petasis, D. T.; Hendrich, M. P. In *Electron Paramagnetic Resonance Investigations of Biological Systems by Using Spin Labels, Spin Probes, and Intrinsic Metal Ions, Pt A*; Qin, P. Z., Warncke, K., Ed.; 2015; Vol. 563, pp 171-208.

(46) Burla, M. C.; Caliandro, R.; Camalli, M.; Carrozzini, B.; Cascarano, G. L.; Giacovazzo, C.; Mallamo, M.; Mazzone, A.; Polidori, G.; Spagna, R. SIR2011: a new package for crystal structure determination and refinement. *J. Appl. Cryst.* **2012,** 45, 357-361.

(47) Frisch, M. J.; Trucks, G. W.; Schlegel, H. B.; Scuseria, G. E.; Robb, M. A.; Cheeseman, J. R.; Scalmani, G.; Barone, V.; Mennucci, B.; Petersson, G. A.; Nakatsuji, H.; Caricato, M.; Li, X.; Hratchian, H. P.; Izmaylov, A. F.; Bloino, J.; Zheng, G.; Sonnenberg, J. L.; Hada, M.; Ehara, M.; Toyota, K.; Fukuda, R.; Hasegawa, J.; Ishida, M.; Nakajima, T.; Honda, Y.; Kitao, O.; Nakai, H.; Vreven, T.; Montgomery, J., J. A.; Peralta, J. E.; Ogliaro, F.; Bearpark, M.; Heyd, J. J.; Brothers, E.; Kudin, K. N.; Staroverov, V. N.; Kobayashi, R.; Normand, J.; Raghavachari, K.; Rendell, A.; Burant, J. C.; Iyengar, S. S.; Tomasi, J.; Cossi, M.; Rega, N.; Millam, J. M.; Klene, M.; Knox, J. E.; Cross, J. B.; Bakken, V.; Adamo, C.; Jaramillo, J.; Gomperts, R.; Stratmann, R. E.; Yazyev, O.; Austin, A. J.; Cammi, R.; Pomelli, C.; Ochterski, J. W.; Martin, R. L.; Morokuma, K.; Zakrzewski, V. G.; Voth, G. A.; Salvador, P.; Dannenberg, J. J.; Dapprich, S.; Daniels, A. D.; Farkas, O.; Foresman, J. B.; Ortiz, J. V.; Cioslowski, J.; Fox, D. J. Gaussian, Inc.: Wallingford CT, 2009.

(48) Casida, M. E. In *Recent Advances in Computational Chemistry*; Chong, D. P., Ed.; World Scientific: New York, 1995; Vol. 1, pp 155-192.

(49) Dennington, I., R.; Keith, T.; Millam, J.; Eppinnett, K.; Hovell, W. L.; Gilliland, R. *GaussView, Semichem, Shawnee Mission, KS.* **2003**,

Synopsis

Structures, physicochemical properties, and reactivity of the whole series of mononuclear copper(II)-halide complexes supported by TMG3tach tridentate ligand consisting with *cis,cis*-1,3,5-triaminocyclohexane (tach) and bulky and strongly electron donating substituent *N,N,N',N'*-tetramethylguanidine (TMG) have been explored to evaluate the structural importance on the spectroscopic and electronic features as well as the reactivity toward C–H bond activation reaction.

TOC graphic

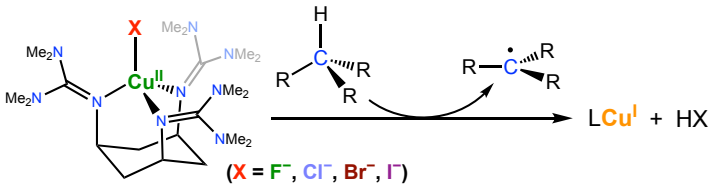

Tetrahedral Cu^II-halide Complexes